Natural Hazards
https://doi.org/10.1007/s11069-025-07145-y

ORIGINAL PAPER

Possible detection of the onset of flash flooding in Thessaly Greece by measurements of the Earth's surface electric field

Efthimios S. Skordas[1] · **Nicholas V. Sarlis**[1] · **Panayiotis A. Varotsos**[1]

Received: 30 October 2024 / Accepted: 20 January 2025

Abstract
Since the beginning of 1980s a telemetric network comprising 18 stations in Greece started to measure remotely the transient electric field changes at the Earth's surface. This article investigates the observed variations of Earth's electric field on 5 September 2023 when the flash flood event occurred at Thessaly Greece as result of storm Daniel. The analyses show that, during the runoffs, the geoelectric field changes abruptly. Such observations could possibly be used as a criterion to estimate the flash flood onset. Upon employing detrended fluctuation analysis at various time scales, we identify three stages corresponding to light (or no) rain, heavy rain, and flood. The distinctive behaviour during the first two stages of the phenomenon under investigation may be used as an early warning. We also show that all stages are governed by fractality.

Keywords Earth's electric field · Flash flood · Runoffs · Seismic electric signal activities

1 Introduction

The Mediterranean region was hit by the storm Daniel between 3 and 8 September 2023. In central Greece an unprecedented meteorological event, occurred and was among the hardest hits by storm in terms of rainfall. According to Hellenic National Meteorological Service, a cumulative height of 350.9 mm of rainfall was received between 4 and 7 September 2023 in Nea Aghialos close to Volos city. For a detailed review of the impact of the storm Daniel in Thessaly Region (Central Greece), see Lekkas et al. (2024).

Since the beginning of 1980s continuous measurements of the electric field variations at the Earth's surface have been made at various sites in Greece, which have been selected after tedious investigation (Varotsos and Alexopoulos 1984a, b). A telemetric network

✉ Efthimios S. Skordas
eskordas@phys.uoa.gr

Nicholas V. Sarlis
nsarlis@phys.uoa.gr

Panayiotis A. Varotsos
pvaro@otenet.gr

[1] Department of Physics, Section of Condensed Matter Physics and Solid Earth Physics Institute, National and Kapodistrian University of Athens, Panepistimiopolis, 157 84 Athens, Greece

of eighteen measuring stations (see Fig. 1 of Varotsos and Alexopoulos (1984a)), was deployed transmitting the data to the central station in Athens (ATH) in real time. The digital data are also saved at the station and nowadays are transmitted to the central station via 4 G GSM (Global System for Mobile communication). Beyond the usual disturbances due to atmospheric or magnetic storms, transient changes of the electric field preceding earthquakes (EQs) (Varotsos and Alexopoulos 1984a, b) have been observed which are called seismic electric signals (SES). The latter appear as transient changes of the potential difference ΔV measured between two electrodes (which are buried at a depth of around 2 m and at distances between them from a few tens of m, short dipole, to several km, long dipole, as described in detail in the next Section). In the case of major EQs, several SES occurring within a short time (termed SES activities) are recorded a few weeks to $5\frac{1}{2}$ months in advance (Varotsos et al. 2011b) (cf. an SES activity enables also the estimation of the epicentral area and the magnitude of the expected EQ, for example, see Fig. 1 that will be also discussed later). One of the measuring stations is located close to Volos city (hereafter labelled VOL). A network of short and long dipoles (see Data and Methods) are deployed in the wide area from Volos to Nea Aghialos, see Fig. 1.4 of (Varotsos et al. 2011b). During the last four decades two SES activities preceding major EQs have been recorded at VOL (Fig. 2): first, an important SES activity was recorded at VOL (cf. its original record shown in Fig. 13.3.1 of Varotsos (2005)) on 30 April 1995 that was followed on 15 June 1995 by the M_w6.5 EQ close to Egion (Peloponnese) (see Sect. 7.2.2 of Varotsos et al. (2011b)). Second, the SES activity depicted in Fig. 19.2 of Lazaridou-Varotsos (2013) on 17 March 2001 also recorded at VOL that preceded the M_w6.5 EQ on 26 July 2001 (Varotsos et al. 2001) close to Skyros island (central Aegean) (cf. In Varotsos et al. (2001) the epicentral area of the expected strong EQ was predicted as shown in Fig. 1 by the black dashed line).

Very recent techniques have been introduced for the timely and accurate identification of seismic electric signals. For example, Xue et al. (2023) developed a real-time automatic search engine (RASE) that incorporates an unsupervised convolutional denoising network module and a supervised long short-term memory (LSTM) prediction network module to automatically search for important SES in real time.

It has been ascertained (Varotsos et al. 2003) that when continuous measurements of both the Earth's electric field and the geomagnetic field are carried out, additional information can be revealed as far as the SES investigation, for example, is concerned. Specifically, Uyeda and Tanaka (2004), based on an article entitled Electric fields that arrive before the time derivative of the magnetic field prior to major-earthquakes by Varotsos et al. (2003), give precise numbers for the time needed to reach from an emitting source (i.e., from an EQ epicentre) to a measuring station. In Varotsos et al. (2003) both electric and magnetic variations (recorded by three coil magnetometers oriented along three axes: EW, NS and vertical) have been measured. It was found that at distances ≈100 km for major earthquakes the electric field arrives 1 to 2 s before the time derivative of the horizontal magnetic field. Such a striking time difference was explained in Varotsos et al. (2003) turning to Maxwell's equations in a cylindrical coordinate system and this is why Uyeda and Tanaka (2004) entitled their article "Maxwell's equations and earthquakes".

Khan et al. (2017a), after reviewing the existing literature on forecasting techniques (Sarkar et al. 2015; Khan et al. 2017b; Suparta et al. 2015; Boni et al. 2009; Zhang et al. 2016; Rohaimi et al. 2016; Macrander et al. 2009; Barrick et al. 2016; Abdelkader et al. 2013; Artigue et al. 2011) approached the investigation of flash floods by observing the geomagnetic field using Tesla meter or magnetometer. Their hourly based reading of magnetometer showed

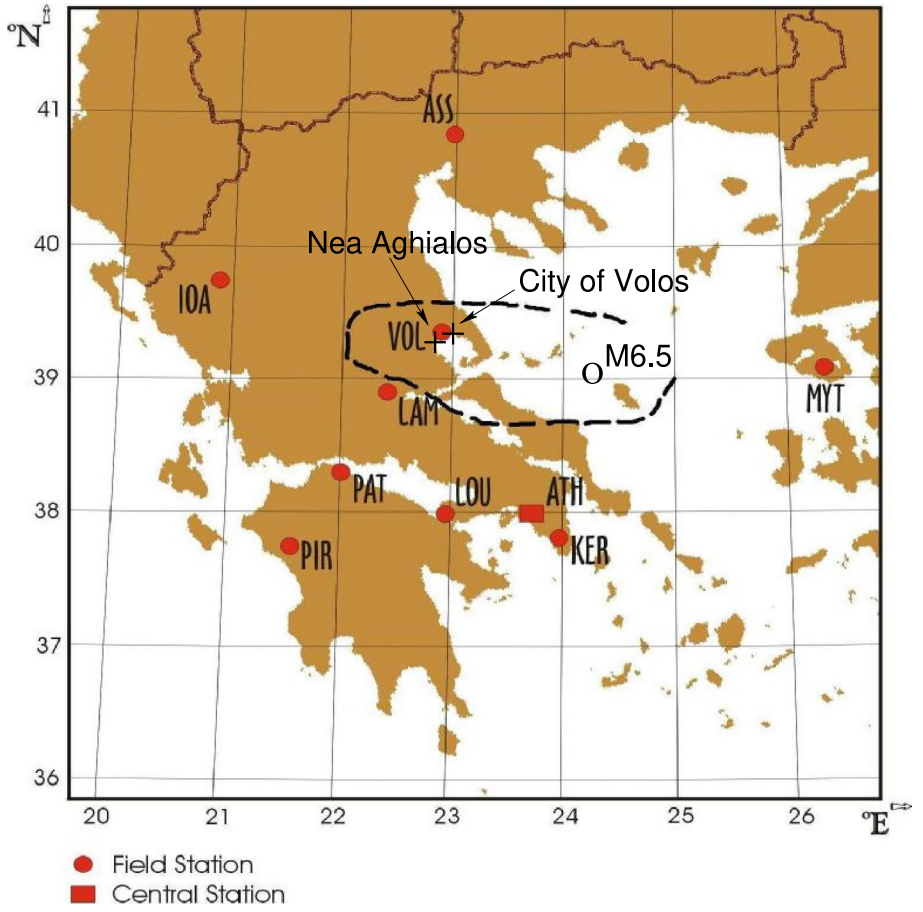

Fig. 1 The map of the fourth page of the manuscript of Varotsos et al. (2001) submitted for publication on 25 March 2001 showing the sites of the nine stations (red dots) of the real time VAN telemetric network being in operation at that time. The black dashed line around VOL indicates the predicted area of the expected EQ. The plus symbols indicate the location of the City of Volos and Nea Aghialos. The epicentre of the *M*6.5 EQ on 26 July 2001 is shown by an open circle

that during the runoffs the geomagnetic field briskly reduced, which can be a yardstick to estimate the flash floods. It is the scope of the present work to investigate the aforementioned flash flood in Thessaly Greece by employing the measurements of the Earth's electric field changes conducted at Volos area.

The present paper is organized as follows: in the next Section, the Data and Methods are summarized. In Sect. 3, the results and their discussion are presented. Finally, Sect. 4 summarizes our findings and concludes the paper.

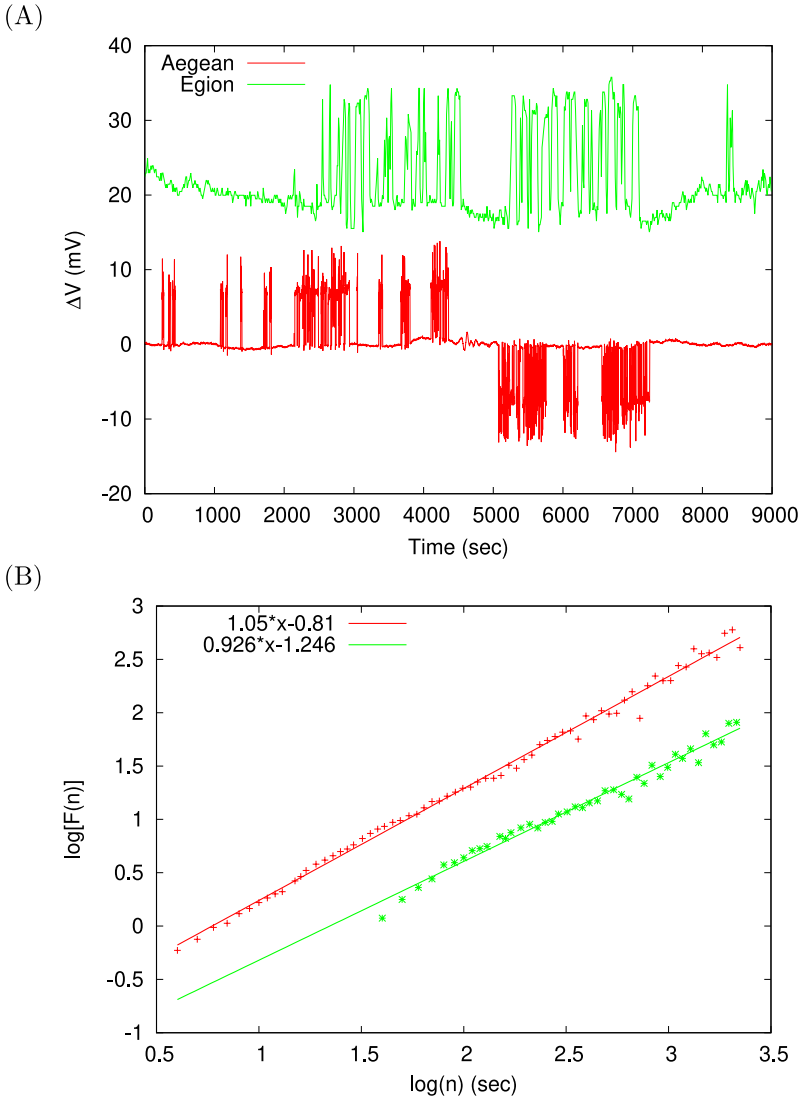

Fig. 2 **A** Recordings of the potential difference ΔV between the electrodes of the long measuring dipole V-$S_{\Sigma B}$ (see Fig. 1.4 of Varotsos et al. (2011b)) from each of the two SES activities, recorded at VOL: on 17 March 2001 preceding the Aegean EQ M_w6.5 on 26 July 2001 (red) (Varotsos et al. 2001) and the one (green) on 30 April 1995 that was followed by the Egion EQ M_w6.5 on 15 June 1995 (see Sect. 7.2.2 of Varotsos et al. (2011b); see also Table 13.3.1 in page 280 of Varotsos (2005)). The sampling rate for the former is 1 sample/s while for the latter is 1 sample/10 s. **B** The DFA exponent has been obtained to be $\alpha =$ 1.05 and 0.926, respectively

2 Data and methods

The electric data presented were recorded by the VAN telemetric network which was set up for the study of SES almost four decades ago in Greece. Such a research was motivated by the detailed study of the thermodynamics of crystal defects in solids (Varotsos

2005) that opened the possibility that rupture in solids could be preceded by transient electric signals. Thus, continuous measurements of the electric field of the Earth have been carried out in Greece since 1982 by the Greek scientists Varotsos, Alexopoulos and Nomicos. This is the reason this method is called VAN method. The telemetric network of eighteen measuring stations via leased telephone lines was completed (Varotsos and Alexopoulos 1984a, b) by 1983 (see Fig. 1 of Varotsos and Alexopoulos (1984a), as mentioned). Data are collected and transmitted in real time(Nomicos and Chatzidiakos 1993; Nomicos et al. 1996; Varotsos 2005) to the central station which is located at a suburb of Athens (ATH). Non-polarizable electrodes $Pb/PbCl_2$ at a depth of 2 m are used and the potential difference between two of them (that constitute a measuring electric dipole) is measured. A minimum of eight measuring electric dipoles was initially installed at each station; some of these dipoles have lengths (L) between 50 m and 400 m and are called short dipoles, while others have appreciably longer lengths (usually between 2 and 20 km) and are called long dipoles. In 1990s, beyond the aforementioned real time data collecting system, dataloggers (Campbell 21X connected to a portable PC) were installed at several stations to collect data with sampling rate $f_s = 1$ sample/s. These data were finally stored only during SES collection, and during the period extending from several minutes before a significant EQ, until a few minutes after. The averages, taken every 20 s (cf. initially it was 1 sample/10 s), were transmitted to the central station (once or twice per day) through dial-up. In 2010s, the dial-up collection was replaced by GSM and the electric field data presented in Fig. 3 come from this method with $f_s = 1$ sample/s. Data presented in Fig. 2 come from the older collection method and this is the reason that two different sampling rates were used.

Short and long measuring electric dipoles are deployed in the wide area of Volos (see Fig. 1.4 of Varotsos et al. (2011b)) for the detection of the anomalous variations of the electric field of the Earth.

The rainfall data and rain duration from Nea Aghialos are provided, upon request, from the Hellenic National Meteorological Service. The data start from 09:00 at 4 September 2023 and a value is reported every 3 h.

In our analysis, we apply the Detrended Fluctuation Analysis (DFA), which was first introduced by Peng et al. (1994) and used to quantify long-range correlation and fractal scaling behaviour in the nonstationary behaviour of time series.

In general, the DFA presents some assets over other traditional methods. For instance, it detects intrinsic self-similarity in many nonstationary time series, especially in those that have a slow trend variation; also it prevents from illusory self-similarity. In the past few years, the DFA method has been used to effectively analyse a variety of time series involving several fields of knowledge, such as DNA (Peng et al. 1994; Mantegna et al. 1994; Buldyrev et al. 1995), cardiac dynamics (Ivanov et al. 1999; Havlin et al. 1999; Stanley et al. 1999), neuronal oscillations (Hardstone et al. 2012), heartbeat fluctuation (Bunde et al. 2000; Ivanov et al. 1998), meteorology (Ivanova et al. 2003), climatology (Varotsos et al. 2013), etc.

The method consists of the following: beginning with a time series or signal $x(i)$, with $i = 1, 2, \ldots, N$ and N the length of the time series, the steps of the DFA method are (e.g., see Varotsos et al. (2023):

1. We first construct the signal profile of the time series by integrating $x(i)$ with respect to its mean $\langle x \rangle$:

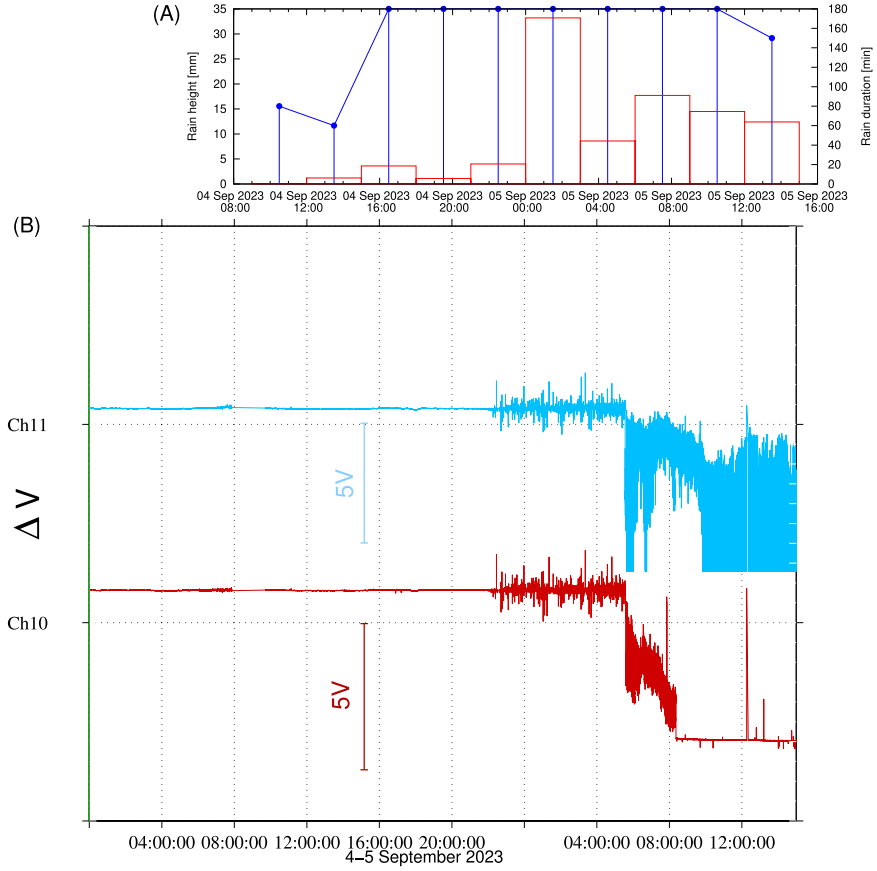

Fig. 3 **A** The rainfall data at Nea Aghialos station of the Hellenic National Meteorological Service until 15:00 UTC on 5 September 2023. The red bars show the rain height in mm (left scale) while the blue line denotes the rain duration in minutes (right scale). The rain height as well as the rain duration are reported every three hours. **B** The recordings of the electric dipoles (ΔV) at VOL station of the VAN telemetric network from 00:00 UTC on 4 September 2023 until 15:00 UTC on 5 September 2023

$$y(i) = \sum_{j=1}^{i} [x(j) - \langle x \rangle] \tag{1}$$

where $\langle x \rangle$ is the mean:

$$\langle x \rangle = \frac{1}{N} \sum_{j=1}^{N} x(j). \tag{2}$$

2. Then the profile $y(i)$ is divided into non-overlapping segments of equal length n. Then, for all segments, a least squares line is fit to the data in the corresponding segment, which represents a local trend in that segment. From the linear fit, we use the y-coordinate to define the local trends, $y_n(i)$.

3. We detrend the profile $y(i)$, by subtracting the local trend, $y_n(i)$, in each one of the segments, i.e., we obtain:

$$Y_n(i) = y(i) - y_n(i). \tag{3}$$

4. The mean squared of the integrated and detrended time series is computed:

$$F(n)^2 \equiv \frac{1}{N}\sum_{i=1}^{N}[Y_n(i)]^2 \tag{4}$$

5. We repeat steps 2, 3, and 4 for each one of the characteristic time scales set in the time series.
6. Finally, we compute a fit between $F(n)$ and the segment size n: $F(n) \propto n^{\alpha}$. The slope of a linear fit between log-rms ($\log[F(n)]$) and log-scales ($\log(n)$) provides the scaling (or DFA) exponent α.

If $\alpha < 0.5$, the signal or time series is anti-correlated; if $\alpha \simeq 0.5$, the signal is uncorrelated (white noise); if $\alpha > 0.5$, the signal is correlated; and if $\alpha \simeq 1$, the signal is $1/f$-noise (pink noise). The results presented below, have been obtained by the DFA (Peng et al. 1994, 1995a) computer code `dfa.c` developed by J. Mietus, C.-K. Peng, and G. Moody available from Physionet (Goldberger et al. 2000).

The following remark is important for the application of DFA: in the beginning of 2000s a new concept of time, the natural time was introduced (Varotsos et al. 2002) and has been shown that unique dynamic features hidden behind can be revealed from the time series of complex systems. In particular, natural time analysis can serve for the discrimination between SES and man made "artificial" noise as well as for a better estimation of the time window between the initiation of an SES activity and an EQ (Varotsos et al. 2011b). Only in natural time analysis DFA can distinguish SES activities from "artificial" (man-made) noises leading to an exponent α close to unity for the SES activities, while $\alpha \approx 0.65 - 0.8$ for artificial noises (see p.210 of Varotsos et al. (2011b)). In addition, although opinions have been expressed that the self-organized criticality should only emerge at continental level (Perinelli et al. 2024), natural time analysis of seismicity reveals that, for example, the normalized power spectrum—defined in natural time (Varotsos et al. 2011b, 2023)—of the Southern California Earthquake Catalog (SCEC), covering part of the San Andreas fault system, and Japan follow a common curve (see, e.g., Fig. 6.4 of, Varotsos et al. (2011b)) in spite of the fact that they are located at different continents. Furthermore, natural time analysis reveals that a common feature emerges for the order parameter fluctuations of seismicity in different correlated systems as for example for the worldwide seismicity, SCEC, Japan etc (Sarlis et al. 2011). Very recently was shown that natural time analysis reveals that before major EQs independent datasets of different geophysical observables (seismicity, Earth's magnetic and/or electric field) exhibit changes, which are observed simultaneously. This reflects that natural time is the correct framework to study EQ precursory phenomena (Varotsos et al. 2024).

3 Results and discussion

The rainfall data together with the electric measurements are shown in Fig. 3. Fig. 3A shows the rainfall height at Nea Aghialos along with the rain duration, while Fig. 3B depicts the recordings of the electrostatic potential difference ΔV at electric dipoles of the

VOL station for the same time period. Three distinct stages could be perceived in the latter figure: the stage at which the ΔV variations are on the average around 40 mV (see also Fig. 4A that shows the aforementioned electric channels at this time period), in almost all channels, and it lasts from 4 September 2023 at 10:00 UTC, when light rain was reported in Fig. 3A, until 22:00 UTC on the same day. At this time period the rain was 0.0–3.6 mm and not continuous (see Fig. 3A). A second stage, at which the electric variation increased almost by one order of magnitude (see also Fig. 4B), and lasted from 4 September 2023 at 22:00 UTC until 5 September 2023 05:00 UTC. The physical reason behind this variation could be attributed to electrochemical noise, which was discussed by Varotsos and Lazaridou (1991). During this time period it was continuously raining and the rain height was also increased by one order of magnitude reaching a value of 33.2 mm between 00:00 and 03:00 UTC on 5 September 2023. (We note that according to the Hellenic National Meteorological Service www.emy.gr (accessed on 20 June 2024) the monthly mean precipitation (rain) height is 38.5 mm.) The third stage is characterized by very high values of ΔV (see also Fig. 4C), larger than 750 mV, at the long electric dipoles that have one of their electrodes located either at Volos city or at Nea Ionia (a town side by side with Volos city). It is most probably the time at which these electrodes were submerged in the water. It should be noted that the highest rain of 114.5 mm was reported between 21:00 and 24:00 on the 5 th of September 2023.

The DFA exponent α is calculated for the electric dipole presented in Fig. 5A, where one of the electrodes is located at Nea Ionia very close to Volos city (the other electrode is located at 39.28° N 22.88° E). The red part of the signal represents the time of light and not continuous rain, while the green and blue colors are for the continuous heavy rain and the third stage period, respectively. The DFA plot of the whole time series of this channel is shown in Fig. 5B. These data could be fit with three straight lines and the corresponding scaling exponents are $\alpha = 1.25$, 0.75 and 1.07 for the short (i.e., smaller than ≈ 50 s), the intermediate (between 50 and 300 s) and the long time lags (≥ 300 s), respectively. Note that the exponent $\alpha = 0.75$ found for the intermediate scale is comparable with the values reported for "artificial" noises when they are analysed in natural time (see p. 210 of Varotsos et al. (2011b)), while the values of $\alpha = 1.25$ for the small time lags indicate non-stationarity. For time lags ≥ 300 s the signal is 1/*f*-noise.

Figure 5C–E depict the DFA plot for the three parts of the electric signal in Fig. 5A related to three different situations concerning the rainfall. The common characteristic in the plots of DFA for the three parts of these electric signals is that the data are not described by a single DFA exponent α as in the case of SES, see Fig. 2B, but a different exponent should be used for the small and the large scales (for the importance of crossovers in DFA see Peng et al. (1995b); Chen et al. (2002); Telesca et al. (2012)). For the first (red) part of the signal in Fig. 5A, with light or no rain, which corresponds to time lags smaller than ~ 50 s $\alpha = 1.08$ indicating 1/*f*-noise, while for time lags > 50 s $\alpha = 1.41$ indicating non-stationarity. The second part (green) of the signal corresponds to heavy rain and the value of α is 0.48 (white noise) and 1.15 (1/*f*-noise) for small and large scales, respectively. The crossover between the two scales is at ~ 250 s. For the blue part of Fig. 5E, the DFA plot shows two scales that cross at ~ 100 s with α values 1.23 and 0.92 for the small and the large scales, respectively.

The appearance of crossovers in Fig. 5 is in sharp contrast to the description of the DFA of the electric field in the case of SES activities, see Fig. 2. There we observe that single DFA exponents close to unity appear indicating an 1/*f* fractal behaviour of noise which is ubiquitous in complex systems as well as in electronic devices, for a recent example see, e.g., (Samara et al. 2023). We emphasize, however, that a clear distinction of SES from

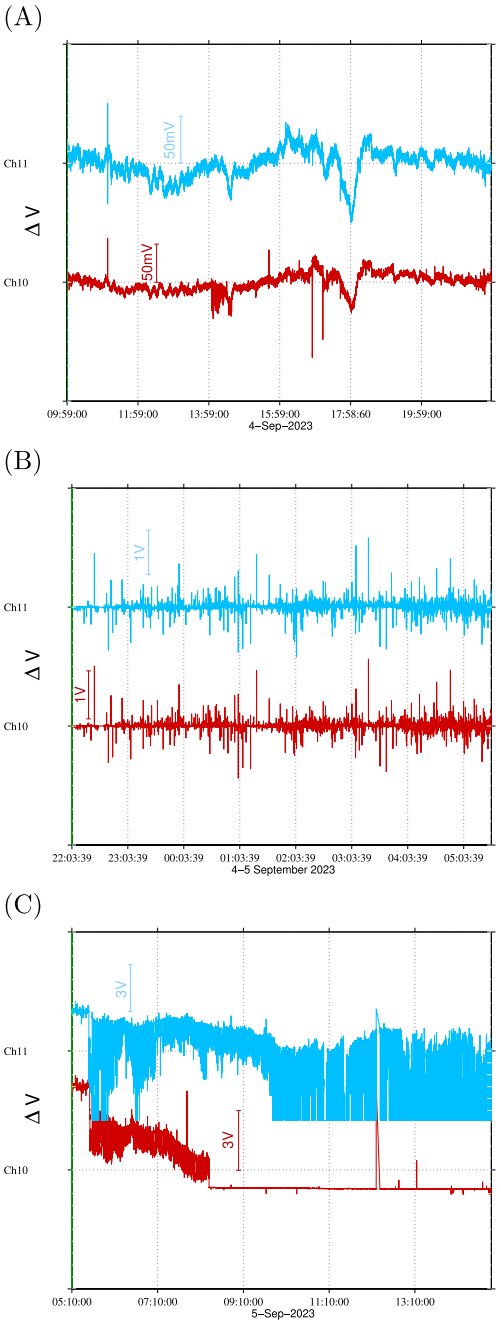

Fig. 4 The recordings of the electric dipoles (ΔV) at VOL depicted in Fig. 3B zoomed at the three stages mentioned in Sect. 3. During **A** the time period from 10:00 to 22:00 UTC on 4 September 2023 that the rain height was 0.0–3.6 mm and not continuous, **B** the time of continuous raining (the rain height was increased by one order of magnitude ≈ 33.2 mm, compared to (**A**)) and **C** the time at which electrodes were submerged in the water

noise is achieved only when analysing the corresponding signals in natural time (Varotsos et al. 2011b, 2009). At this point, we have to note that very recently Perinelli et al. (2024) studied the fractality of EQs and found results compatible with those obtained by natural time analysis and earthquake nowcasting (Varotsos et al. 2021).

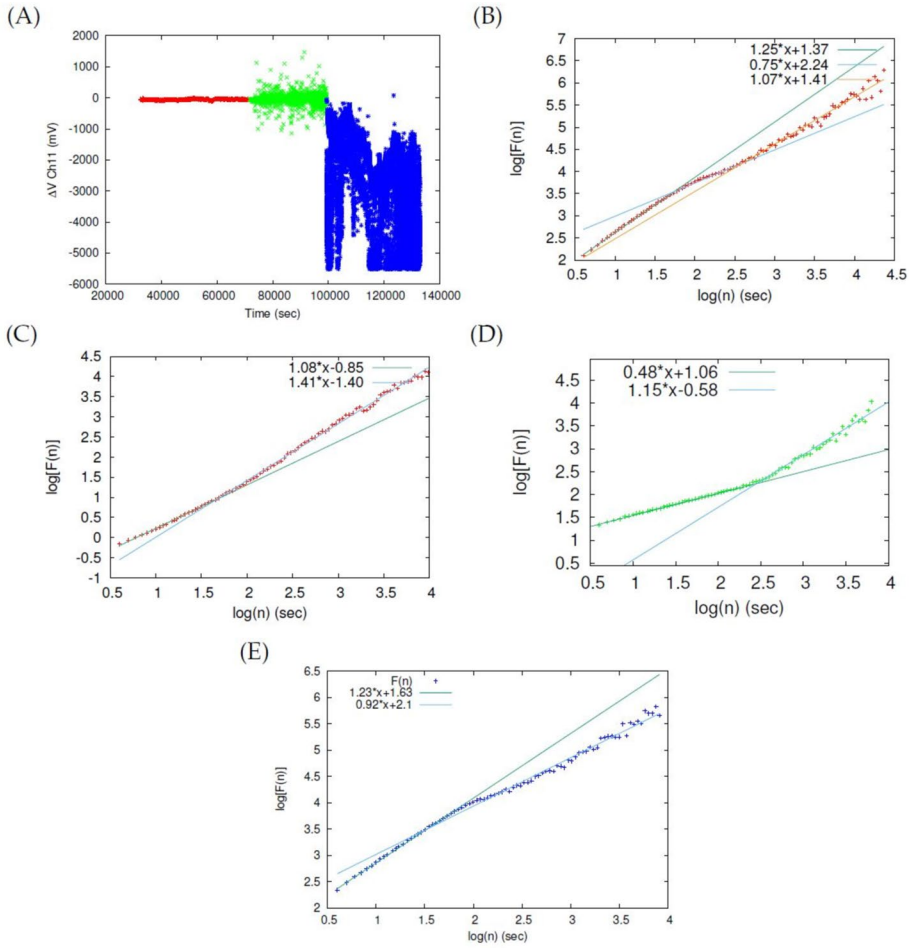

Fig. 5 **A** The electric channel 11 (see Fig. 4) used in the DFA analysis: the red, green, and blue points correspond to the data depicted in Fig. 4A–C, respectively. The DFA for: **B** the whole record shown in (**A**), where three scales are observed with DFA exponent $\alpha = 1.25$ for the small scales $\alpha = 0.75$ for the intermediate scales and $\alpha = 1.07$ for the large scales. **C** The first part of the signal (red portion in (A)). Two scales are observed with $\alpha = 1.08$ and 1.41 for the small and the large scales, respectively. **D** The middle part of the record (green portion in (**A**)). Two scales are observed with $\alpha = 0.48$ for the small scales and $\alpha = 1.15$ for the large scales. **E** The last part of the record (blue portion in (**A**)) where again two scales are observed with $\alpha = 1.23$ and 0.92 for small and large scales, respectively

Another important point to be mentioned is the difference between the values of the DFA exponents α at the short scales during the first stage, see Fig. 5C, and the second stage, see Fig. 5D. By studying all the channels depicted in Fig. 3, we verified that during the first stage (light rain), for short scales $n < 50$ s, $\alpha \approx 1.0$ while during the second stage (heavy rain), the corresponding DFA exponent for short scales ($n < 250$ s) falls to $\alpha \approx 0.5$. Interestingly, such a transition from persistent behaviour to almost random behaviour is also observed in a variety of critical phenomena including EQs or sudden

cardiac death, see Varotsos et al. (2023). This is of key importance because it can serve as precursory stage for an impending flash flood.

In order to examine if a similar phenomenon was observed in a previous case, we studied the records of the VAN network on 9 October 2006, when a flash flood hit the city of Volos (Papaioannou et al. 2019). Figure 6 depicts the records of channels 9 and 10 of VOL geoelectric station on 9 October 2006. If we analyse by means of DFA the variations of the potential difference before these two channels were led to saturation, we obtain the results shown in Fig. 7. In the latter figure we observe significantly smaller α values for the shorter scales. This is in accordance with the aforementioned observation of $\alpha \approx 0.5$ for the short scales, during heavy rain, pointing to the importance of this phenomenon as precursory stage for an impending flash flood. Additionally, the duration of this precursory phenomenon which is 7 h before the 5 September 2023 flash flood and 6 h before the 9 October 2006 flash flood allows the early warning with respect to aims of civil protection.

Scaling is used in order to unify spatial scaling flood statistics with physical processes for solving the global problem of prediction of floods from ungauged and poorly gauged basins (Gupta 2004). As stated by Gupta (2004), a mathematical framework has been developed to predict the scaling parameters from space-time variable physical processes so that the corresponding empirical values of these parameters can be understood and

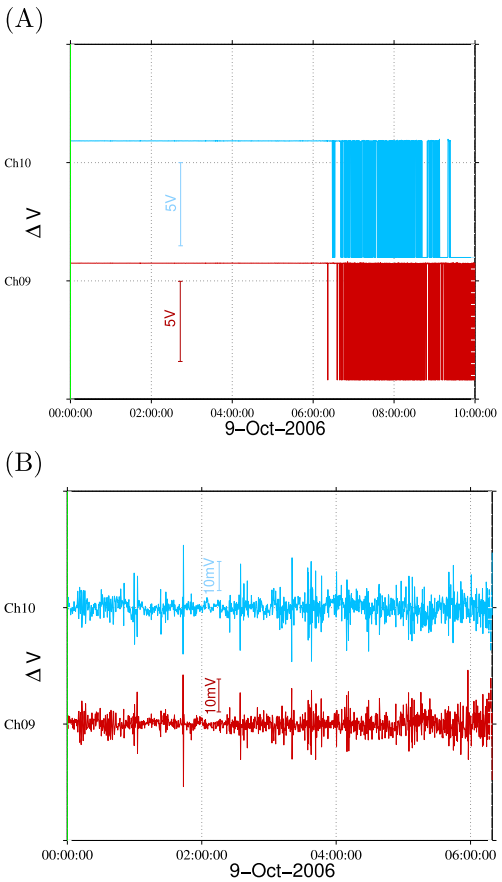

Fig. 6 **A** Recordings of the electric dipoles of the VOL station of the VAN network on 9 October 2006. Panel **B** is an excerpt of (**A**) before the saturation of the channels due to the flash flood

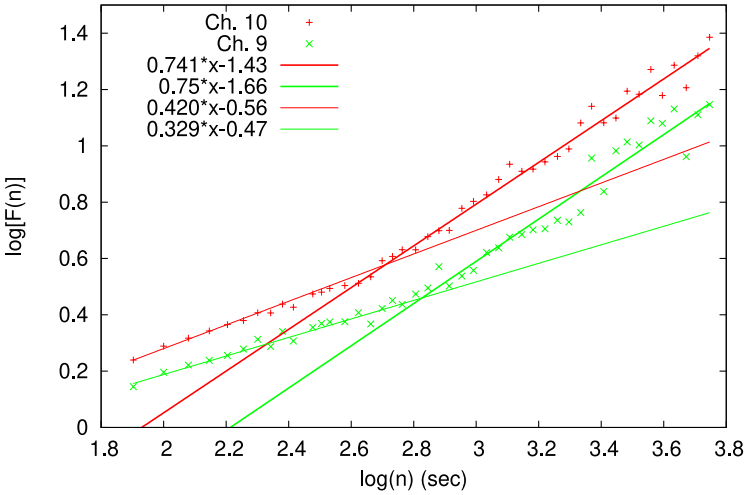

Fig. 7 The DFA of the potential difference depicted in Fig. 6B. Two scales are observed for each channel with the smaller exponent α in the range 0.329–0.420 corresponding to the shorter scales

predicted physically, see also Gupta et al. (1996); Gupta and Waymire (1998); Menabde et al. (2001); Veitzer and Gupta (2001). Medhi and Tripathi (2015) proposes a methodology for exploring the relationship between flood scaling exponents and physical attributes of a river basin by using observed data. Very recently Mazivanhanga et al. (2024) found that peak discharge in the La Sierra catchment exhibits powerlaw relationships. Other recent studies on scaling laws have demonstrated the potential of estimating flood parameters by analysing the physical characteristics of drainage areas e.g., Zheng et al. (2021); Medhi and Tripathi (2015); Gupta (2017); Formetta et al. (2021); Gupta et al. (2010); Ayalew et al. (2015, 2018).

The atmospheric electric field has been also used as a precursor for various meteorological parameters. For example, Bernard et al. (2020) investigated the atmospheric electric field derivative frequency distribution prior to bursts of intense rainfall in the Dolomite Alps near Cortina d'Ampezzo, Italy. They designed a regression model which considers the amplitude maximum and the difference in time between the crossings of the electric field derivatives of the zero axis. Their model suggests a mild relationship between electric field and rainfall intensity in an alpine environment. Okubo et al. (2006) found that a strong correlation between the instantaneous fluctuations of atmospheric electric field and the wind speed in the convenient meteorological environment, while Bennett and Harrison (2007) say that changes in the weather are often associated with pronounced changes in mean and variability of the Potential Gradient as noted originally by early workers in atmospheric electricity.

The results presented above suggest that heavy rain may affect the electrical signals SES that are recorded by the VAN network for the prediction of EQs. This is well known for the case of Greece, see e.g. Varotsos and Lazaridou (1991); Varotsos et al. (1993) and has been treated by the use of multiple measuring dipoles using independent electrodes, which are not expected to flood simultaneously except for the cases of extreme flash floods treated here. During the latter cases we have inevitably an interruption of SES monitoring. As shown, however, by Skordas et al. (2010) and Varotsos et al. (2011a) even a significant data

loss does not affect the ability to detect SES before strong EQs upon employing natural time and DFA. Such techniques could be also applied when employing VAN method for predicting EQs in tropical countries during rainy season.

The above indicate that the installation of multiple measuring electric dipoles using independent electrodes and the continuous monitoring of their recordings by DFA (which can be easily automated) has the potential to provide automatic early warning for extreme hydrometeorological phenomena. Such an application involves, of course, a careful selection of the electrode sites at which the electric field on ground surface will be measured and monitored continuously by studying DFA. Electrode sites close to riverbanks or streams which are likely to flood during heavy rain should be preferred and for DFA the recorded data should be analysed every few hours, see, e.g., Figs. 5D and 7. For example, in the case of the recent catastrophic flood in Valencia Spain on 29 October 2024 NASA (2024) if we had applied this method of monitoring DFA of the electric channels, we could possibly have obtained an automatic early warning.

4 Summary and conclusions

In summary, analysing the Earth's electric field data recorded during the storm Daniel at the wide area of Volos, by using the DFA analysis, we found different scaling exponents for the light rain, the heavy rain and the flood periods. This method may provide a new scientific framework for solving the problem of prediction of floods.

In particular, the DFA analysis of the Earth's surface electric field data at VOL station during the storm Daniel in Thessaly, the following interesting characteristics emerge: first, before the beginning of heavy rain the DFA exponent α for short scales is close to unity. Second, this DFA exponent turns to around 0.5 (random behaviour) during the heavy rain. This could be considered as precursory stage of an impending flash flood. Third, when the flood started, abruptly very large ΔV values have been observed and the DFA exponent α turned to $\alpha > 1$.

Note that the above characteristics have been observed at VOL station (which is located at a village outside Volos) earlier than the flash flood hit the main part of Volos city. It is interesting that the above findings have been obtained by means of DFA that can be very easily implemented in online signal analysis methods operating for the prediction of floods.

The first two characteristics stating that from the beginning of heavy rain the DFA exponent turns from unity at short scales to 0.5 during heavy rain is strikingly reminiscent of the following fact: such a transition from a persistent behaviour to almost random behaviour has been observed in various critical phenomena such as earthquakes and sudden cardiac death (Varotsos et al. 2023).

Acknowledgements The authors acknowledge the rain data provided from the Hellenic National Meteorological Service from Nea Aghialos station upon request. We gratefully acknowledge the continuous supervision and technical support of the geoelectrical stations of the VAN telemetric network by Vasilis Dimitropoulos, Spyros Tzigkos and George Lampithianakis.

Author contributions Efthimios S. Skordas: Conceptualization, Methodology, Formal analysis, Investigation, Writing—Original draft preparation, Writing—Reviewing and Editing, Supervision, Project administration. Nicholas V. Sarlis: Conceptualization, Methodology, Software, Formal analysis, Investigation, Resources, Writing—Original draft preparation, Writing—Reviewing and Editing, Visualization. Panayiotis A. Varotsos: Conceptualization, Methodology, Software, Formal analysis, Investigation, Resources, Data curation, Writing—Original draft preparation, Writing—Reviewing and Editing, Visualization.

Funding The authors did not receive support from any organization for the submitted work.

Data availability The data that support the findings of this study are available from the corresponding author upon reasonable request.

Code availability The codes used in this study are available from the corresponding author upon reasonable request.

Declarations

Conflict of interest The authors declare that they have no known competing financial interests or personal relationships that could have appeared to influence the work reported in this paper.

Ethical approval N/A

Consent to participate N/A

Consent for publication N/A

References

Abdelkader M, Shaqura M, Claudel CG, et al (2013) A UAV based system for real time flash flood monitoring in desert environments using lagrangian microsensors. In: 2013 international conference on unmanned aircraft systems (ICUAS), pp 25–34. https://doi.org/10.1109/ICUAS.2013.6564670

Artigue G, Johannet A, Borrell V, et al (2011) Flash floods forecasting without rainfalls forecasts by recurrent neural networks. Case study on the Mialet Basin (Southern France). In: 2011 third world congress on nature and biologically inspired computing, pp 303–310. https://doi.org/10.1109/NaBIC.2011.6089612

Ayalew T, Krajewski W, Mantilla R et al (2018) Can floods in large river basins be predicted from floods observed in small subbasins? J Flood Risk Manag 11(3):331–338. https://doi.org/10.1111/jfr3.12327

Ayalew TB, Krajewski WF, Mantilla R (2015) Analyzing the effects of excess rainfall properties on the scaling structure of peak discharges: insights from a mesoscale river basin. Water Resour Res 51(6):3900–3921. https://doi.org/10.1002/2014WR016258

Barrick D, Lipa B, Isaacson J (2016) Simulator to evaluate tsunami warning performance for coastal hf radars. In: OCEANS 2016 MTS/IEEE monterey, pp 1–5. https://doi.org/10.1109/OCEANS.2016.7761447

Bennett AJ, Harrison RG (2007) Atmospheric electricity in different weather conditions. Weather 62(10):277–283. https://doi.org/10.1002/wea.97

Bernard M, Underwood SJ, Berti M et al (2020) Observations of the atmospheric electric field preceding intense rainfall events in the Dolomite Alps near Cortina d'Ampezzo, Italy. Meteorol Atmos Phys 132:99–111. https://doi.org/10.1007/s00703-019-00677-6

Boni G, Candela L, Castelli F, et al (2009) The OPERA project: EO-based flood risk management in Italy. In: 2009 IEEE international geoscience and remote sensing symposium, pp II–929–II–932. https://doi.org/10.1109/IGARSS.2009.5418250

Buldyrev SV, Goldberger AL, Havlin S et al (1995) Long-range correlation properties of coding and noncoding DNA sequences: Genbank analysis. Phys Rev E 51:5084–5091

Bunde A, Havlin S, Kantelhardt JW et al (2000) Correlated and uncorrelated regions in heart-rate fluctuations during sleep. Phys Rev Lett 85:3736–3739. https://doi.org/10.1103/physrevlett.85.3736
Chen Z, Ivanov PC, Hu K et al (2002) Effect of nonstationarities on detrended fluctuation analysis. Phys Rev E 65:041107. https://doi.org/10.1103/PhysRevE.65.041107
Formetta G, Over T, Stewart E (2021) Assessment of peak flow scaling and its effect on flood quantile estimation in the United Kingdom. Water Resour Res 57(4):e2020WR028076. https://doi.org/10.1029/2020WR028076
Goldberger AL, Amaral LAN, Glass L, et al (2000) Physiobank, physiotoolkit, and physionet-components of a new research resource for complex physiologic signals. Circulation 101:E215 (see also www.physionet.org) [SPACE]https://doi.org/10.1161/01.CIR.101.23.e215
Gupta V (2017). Scaling theory of floods for developing a physical basis of statistical flood frequency relations. https://doi.org/10.1093/acrefore/9780199389407.013.301
Gupta VK (2004) Emergence of statistical scaling in floods on channel networks from complex runoff dynamics. Chaos, Solitons Fractals 19(2):357–365. https://doi.org/10.1016/S0960-0779(03)00048-1
Gupta VK, Waymire EC (1998) Scale dependence and scale invariance in hydrology: spatial variability and scale invariance in hydrologic regionalization. In: Proceedings of the scale dependence and scale invariance in Hydrology. https://api.semanticscholar.org/CorpusID:129351266
Gupta VK, Castro SL, Over TM (1996) On scaling exponents of spatial peak flows from rainfall and river network geometry. J Hydrol 187(1):81–104. https://doi.org/10.1016/S0022-1694(96)03088-0
Gupta VK, Mantilla R, Troutman BM et al (2010) Generalizing a nonlinear geophysical flood theory to medium-sized river networks. Geophys Res Lett. https://doi.org/10.1029/2009GL041540
Hardstone R, Poil SS, Schiavone G et al (2012) Detrended fluctuation analysis: a scale-free view on neuronal oscillations. Front Physiol 3:450. https://doi.org/10.3389/fphys.2012.00450
Havlin S, Buldyrev SV, Bunde A et al (1999) Scaling in nature: from DNA through heartbeats to weather. Phys A 273:46
Ivanov PC, Nunes Amaral LA, Goldberger AL et al (1998) Stochastic feedback and the regulation of biological rhythms. Europhys Lett 43:363
Ivanov PC, Rosenblum MG, Peng CK et al (1999) Multifractality in human heartbeat dynamics. Nature 399:461
Ivanova K, Ackerman TP, Clothiaux EE et al (2003) Time correlations and 1/f behavior in backscattering radar reflectivity measurements from cirrus cloud ice fluctuations. J Geophys Res Atmos 108:D9. https://doi.org/10.1029/2002JD003000
Khan T, Kadir K, Alcm M, et al (2017a) Geomagnetic field measurement at earth surface: flash flood forecasting using tesla meter. In: 2017 international conference on engineering technology and technopreneurship (ICE2T), pp 1–4. https://doi.org/10.1109/ICE2T.2017.8215991
Khan TA, Alam M, Shahid Z, et al (2017b) Prior investigation for flash floods and hurricanes, concise capsulization of hydrological technologies and instrumentation: a survey. In: 2017 IEEE 3rd International conference on engineering technologies and social sciences (ICETSS), pp 1–6. https://doi.org/10.1109/ICETSS.2017.8324170
Lazaridou-Varotsos MS (2013) Earthquake prediction by seismic electric signals. The success of the VAN method over thirty years, Springer-Verlag, Berlin. https://doi.org/10.1007/978-3-642-24406-3
Lekkas E, Diakakis M, Mavroulis S et al (2024) The early September 2023 Daniel storm in Thessaly region (Central Greece). Newslett Environ, Disast Crises Manag Strateg 30:1–212
Macrander A, Gouretski V, Boebel O (2009) Pact-a bottom pressure based, compact deep-ocean tsunameter with acoustic surface coupling. In: OCEANS 2009-EUROPE, pp 1–5. https://doi.org/10.1109/OCEANSE.2009.5278247
Mantegna RN, Buldyrev SV, Goldberger AL et al (1994) Linguistic features of noncoding DNA sequences. Phys Rev Lett 73:3169–3172
Mazivanhanga C, Grabowski RC, Perez-Sanchez E et al (2024) Analysis of scaling relationships for flood parameters and peak discharge estimation in a tropical region. Hydrol Res 55(2):161–179. https://doi.org/10.2166/nh.2024.111
Medhi H, Tripathi S (2015) On identifying relationships between the flood scaling exponent and basin attributes. Chaos Interdiscip J Nonlinear Sci 25(7):075405. https://doi.org/10.1063/1.4916378
Menabde M, Veitzer S, Gupta V et al (2001) Tests of peak flow scaling in simulated self-similar river networks. Adv Water Resour 24(9):991–999. https://doi.org/10.1016/S0309-1708(01)00043-4
National Aeronautics and Space Administration (NASA) Earth Observatory (2024) Valencia floods. Available online at https://earthobservatory.nasa.gov/images/153533/valencia-floods
Nomicos K, Chatzidiakos P (1993) A telemetric system for measuring electrotelluric variations in Greece and its application to earthquake prediction. Tectonophysics 224:39–46

Nomicos K, Makris J, Kefalas M (1996) The telemetric system of VAN group, in the critical review of VAN: earthquake prediction from seismic electric signals. In: Lighthill JS (ed) The critical review of VAN: earthquake prediction from seismic electric signals. World Scientific, Singapore, p 77

Okubo K, Chida M, Nobunao T (2006) Analysis of atmospheric electric field variation signals using digital natural observation method. Electr Eng Jpn 155:450–456. https://doi.org/10.1002/eej.20302

Papaioannou G, Varlas G, Terti G et al (2019) Flood inundation mapping at ungauged basins using coupled hydrometeorological-hydraulic modelling: the catastrophic case of the 2006 flash flood in Volos City, Greece. Water 11(11):2328. https://doi.org/10.3390/w11112328

Peng CK, Buldyrev SV, Havlin S et al (1994) Mosaic organization of DNA nucleotides. Phys Rev E 49:1685–1689. https://doi.org/10.1103/physreve.49.1685

Peng CK, Buldyrev SV, Goldberger AL et al (1995) Statistical properties of DNA sequences. Phys A 221:180–192. https://doi.org/10.1016/0378-4371(95)00247-5

Peng CK, Havlin S, Stanley HE et al (1995) Quantification of scaling exponents and crossover phenomena in nonstationary heartbeat time series. Chaos 5:82–87. https://doi.org/10.1063/1.166141

Perinelli A, Ricci L, De Santis A et al (2024) Earthquakes unveil the global-scale fractality of the lithosphere. Commun Earth Environ 5:146. https://doi.org/10.1038/s43247-023-01174-w

Rohaimi NA, Ruslan FA, Adnan R (2016) 3 hours ahead of time flood water level prediction using NNARX structure: case study pahang. In: 2016 7th IEEE control and system graduate research colloquium (ICSGRC), pp 98–103. https://doi.org/10.1109/ICSGRC.2016.7813309

Samara G, Vasileiadis N, Mavropoulis A, et al (2023) 1/f and random telegraph noise of single-layer graphene devices with interdigitated electrodes. In: 2023 international conference on noise and fluctuations (ICNF), pp 1–4. https://doi.org/10.1109/ICNF57520.2023.10472775

Sarkar S, Damarla T, Ray A (2015) Real-time activity recognition from seismic signature via multi-scale symbolic time series analysis (MSTSA). In: 2015 American control conference (ACC), pp 5818–5823. https://doi.org/10.1109/ACC.2015.7172251

Sarlis NV, Skordas ES, Varotsos PA (2011) Similarity of fluctuations in systems exhibiting self-organized criticality. EPL 96:28006. https://doi.org/10.1209/0295-5075/96/28006

Skordas ES, Sarlis NV, Varotsos PA (2010) Effect of significant data loss on identifying electric signals that precede rupture estimated by detrended fluctuation analysis in natural time. Chaos 20:033111

Stanley HE, Nunes Amaral LA, Goldberger AL et al (1999) Statistical physics and physiology: monofractal and multifractal approaches. Phys A 270:309

Suparta W, Rahman R, Singh MSJ et al (2015) Investigation of flash flood over the West Peninsular Malaysia by global positing system network. Adv Sci Lett 21(2):153–157. https://doi.org/10.1166/asl.2015.5845

Telesca L, Pierini JO, Scian B (2012) Investigating the temporal variation of the scaling behavior in rainfall data measured in central Argentina by means of detrended fluctuation analysis. Physica A 391:1553–1562. https://doi.org/10.1016/j.physa.2011.08.042

Uyeda S, Tanaka H (2004) Maxwell's equations and earthquakes. Phys World 17(2):21–22. https://doi.org/10.1088/2058-7058/17/2/30

Varotsos C, Melnikova I, Efstathiou MN et al (2013) 1/f noise in the UV solar spectral irradiance. Theor Appl Climatol 111:641–648. https://doi.org/10.1007/s00704-012-0697-8

Varotsos P (2005) The physics of seismic electric signals. TERRAPUB, Tokyo

Varotsos P, Alexopoulos K (1984) Physical properties of the variations of the electric field of the earth preceding earthquakes, I. Tectonophysics 110:73–98. https://doi.org/10.1016/0040-1951(84)90059-3

Varotsos P, Alexopoulos K (1984) Physical properties of the variations of the electric field of the earth preceding earthquakes, II. Tectonophysics 110:99–125. https://doi.org/10.1016/0040-1951(84)90060-X

Varotsos P, Lazaridou M (1991) Latest aspects of earthquake prediction in Greece based on seismic electric signals. Tectonophysics 188:321–347. https://doi.org/10.1016/0040-1951(91)90462-2

Varotsos P, Alexopoulos K, Lazaridou M (1993) Latest aspects of earthquake prediction in Greece based on seismic electric signals, II. Tectonophysics 224:1–37. https://doi.org/10.1016/0040-1951(93)90055-O

Varotsos P, Sarlis N, Skordas E (2001) A note on the spatial extent of the Volos SES sensitive site. Acta Geophys Pol 49:425–435

Varotsos P, Sarlis N, Skordas E (2011) Identifying long-range correlated signals upon significant periodic data loss. Tectonophysics 503:189–194. https://doi.org/10.1016/j.tecto.2011.02.011

Varotsos PA, Sarlis NV, Skordas ES (2002) Long-range correlations in the electric signals that precede rupture. Phys Rev E 66:011902. https://doi.org/10.1103/physreve.66.011902

Varotsos PA, Sarlis NV, Skordas ES (2003) Electric fields that "arrive'' before the time derivative of the magnetic field prior to major earthquakes. Phys Rev Lett 91:148501. https://doi.org/10.1103/PhysRevLett.91.148501

Varotsos PA, Sarlis NV, Skordas ES (2009) Detrended fluctuation analysis of the magnetic and electric field variations that precede rupture. Chaos 19:023114. https://doi.org/10.1063/1.3130931

Varotsos PA, Sarlis NV, Skordas ES (2011) Natural time analysis: the new view of time. Precursory seismic electric signals, earthquakes and other complex time-series, Springer-Verlag, Berlin. https://doi.org/10.1007/978-3-642-16449-1

Varotsos PA, Sarlis NV, Skordas ES (2023) Natural time analysis: the new view of time, Part II. Advances in disaster prediction using complex systems. Springer Nature, Cham. https://doi.org/10.1007/978-3-031-26006-3

Varotsos PA, Sarlis NV, Skordas ES (2024) Direct interconnection of seismicity with variations of the earth's electric and magnetic field before major earthquakes. Europhys Lett 146(2):22001. https://doi.org/10.1209/0295-5075/ad37d6

Varotsos PK, Perez-Oregon J, Skordas ES et al (2021) Estimating the epicenter of an impending strong earthquake by combining the seismicity order parameter variability analysis with earthquake networks and nowcasting: application in Eastern Mediterranean. Appl Sci 11(21):10093. https://doi.org/10.3390/app112110093

Veitzer SA, Gupta VK (2001) Statistical self-similarity of width function maxima with implications to floods. Adv Water Resour 24(9):955–965. https://doi.org/10.1016/S0309-1708(01)00030-6

Xue J, Wu S, Huang Q et al (2023) Rase: a real-time automatic search engine for anomalous seismic electric signals in geoelectric data. IEEE Trans Geosci Remote Sens 61:1–11. https://doi.org/10.1109/TGRS.2023.3260202

Zhang S, Lu L, Yu J, et al (2016) Short-term water level prediction using different artificial intelligent models. In: 2016 fifth international conference on agro-geoinformatics (Agro-Geoinformatics), pp 1–6. https://doi.org/10.1109/Agro-Geoinformatics.2016.7577678

Zheng Y, Li J, Zhang T et al (2021) Exploring the application of flood scaling property in hydrological model calibration. J Hydrometeorol 22(12):3255–3274. https://doi.org/10.1175/JHM-D-21-0123.1